Acta Materialia 236 (2022) 118115

Contents lists available at ScienceDirect

Acta Materialia

journal homepage: www.elsevier.com/locate/actamat

Full length article

Flexible polarization configuration in high-entropy piezoelectrics with high performance

Ye Liu[a,1], Jiyuan Yang[b,1], Shiqing Deng[a,c,d,1,*], Yueyun Zhang[a], Yongcheng Zhang[e], Shengdong Sun[a], Lu Wang[a], Xiaodong Jiang[e], Chuanrui Huo[a], Hui Liu[c], He Qi[a,*], Shi Liu[b,f,*], Jun Chen[a,*]

[a] Beijing Advanced Innovation Center for Materials Genome Engineering, Department of Physical Chemistry, University of Science and Technology Beijing, Beijing 100083, China
[b] Key Laboratory for Quantum Materials of Zhejiang Province, Department of Physics, School of Science, Westlake University, Hangzhou, Zhejiang, 310024, China
[c] School of Mathematics and Physics, University of Science and Technology Beijing, Beijing, China
[d] State Key Laboratory of New Ceramic and Fine Processing, Tsinghua University, Beijing 100084, China
[e] College of Physics, Center for Marine Observation and Communications, Qingdao University, Qingdao 266071, China
[f] Institute of Natural Science, Westlake Institute for Advanced Study, Hangzhou, Zhejiang 310024, China

ARTICLE INFO

Article history:
Received 21 February 2022
Revised 25 May 2022
Accepted 22 June 2022
Available online 23 June 2022

Keywords:
Piezoelectrics
Polarization configuration
Atomic statistical analysis
Polarization rotation
In-situ SXRD
High entropy

ABSTRACT

Polarization configuration engineering by compositional and structural tuning in piezoelectrics holds great promise for high piezoelectricity that benefits wide electromechanical applications. Here, a novel flexible polarization configuration is achieved in high-entropy Pb-based perovskites, which contributes to superior piezoelectricity of d_{33} ~1200 pC/N. Emergent characteristics and behaviors of such a flexible polarization configuration are thoroughly investigated by the combination of atomic-scale scanning transmission electron microscopy, *in-situ* high-energy synchrotron X-ray diffraction, and first-principles calculations. The multiple interactions among the *A* and *B*-site atoms, originating from the increase of the species of *B*-site elements as well as the enhanced entropy of the system, weaken the long-range polarization order, enhance the flexibility of the polarization under the external field, and eventually result in the high piezoelectric performance. This work demonstrates that polarization configuration engineering through the high-entropy method would be an effective strategy for obtaining outstanding piezoelectric properties, which provides new opportunities for the design and discovery of high-performance piezoelectrics.

1. Introduction

As an important kind of functional material, piezoelectric ceramics have been extensively applied in various electromechanical fields, such as sensors and actuators, where high piezoelectricity is the key to high-efficient energy conversation or detection. From the microscopic aspect, the piezoelectric performance (d_{33}) essentially depends on the characteristics of the polarization. This, therefore, makes the adjustment of polarization an effective path for achieving high performance [1–4]. To realize the appropriate adjustment of polarization, one of the most representative strategies should belong to the construction of phase boundaries that include the morphotropic phase boundary (MPB) and the polymorphic phase boundary (PPB) [1,5]. This is because, at the MPB or PPB, the phase structure is considered as the coexistence of different ferroelectric phases [2,3] or the appearance of a monoclinic phase [11–13]. Multiple phases coexisting with diversity in polarization can smooth the free energy profile and the monoclinic phase can be the "bridge" among polarizations during the reorientation process due to its special polarization orientation [14,15]. Both factors can enhance the mobility of polarization and lead to high piezoelectric performance. For example, many classic piezoelectrics, such as $Pb(Zr,Ti)O_3$ (PZT) [1], $Pb(Mg,Nb)O_3$-$PbTiO_3$ [5], $(Bi,Na)TiO_3$-$BaTiO_3$ [6], and $BiFeO_3$-$PbTiO_3$ [7], were originally designed according to constructing MPB [1,8]. As to the construction of PPB, the enhancement of piezoelectric properties is generally contributed by the shift of the phase transition temperatures to room temperature [9]. Typical examples include the rhombohedral-orthorhombic-tetragonal (*R*-*O*-*T*) phase boundary in

* Correspondence authors.
E-mail addresses: sqdeng@ustb.edu.cn (S. Deng), qiheustb@ustb.edu.cn (H. Qi), liushi@westlake.edu.cn (S. Liu), junchen@ustb.edu.cn (J. Chen).
[1] Y. Liu, J. Yang and S. Deng contributed equally to this work.

https://doi.org/10.1016/j.actamat.2022.118115
1359-6454/

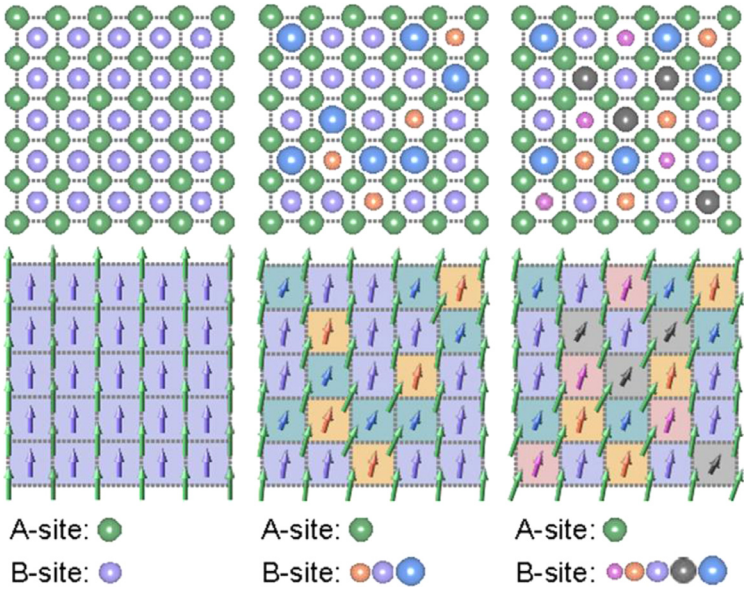

Fig. 1. Schematic of the concept of high-entropy piezoelectrics (HEPs), showing the influence of *B*-site element diversity on the polarization distribution (indicated by arrows in the lower panel) of PbBO_3-based solid solutions.

potassium sodium niobate-based piezoelectrics [10] and the triple point in Ba(Zr,Ti)O_3-(Ba,Ca)TiO_3 [2]. Moreover, recent studies reported that by constructing local structural heterogeneity in relaxor ferroelectrics the ultra-high piezoelectricity [4,16] could also be achieved due to the significant increase in the polarization mobility, which was induced by the similar-sized polar nano regions and high-density randomly distributed nano domain walls. In this sense, one can notice that no matter the strategies of phase boundary, monoclinic phase, or local structural heterogeneity, the key essence is alike, that is, modulating the local behavior of the polarization, including its diversity, flexibility, and mobility. This essentially underscores the critical role of the configuration of polarization and implies that appropriately modulated polarization configurations through new design ideas can promisingly yield superior piezoelectric properties.

To achieve a high flexible polarization configuration, the long-rang ordering of polarization should be broken, and the local polarization ordering should be perturbed as much as possible, for example, by enhancing the contributions from nano domain walls in the polarization configuration at MPB. Generally, the unary systems of perovskite (ABO_3) with a single element at the *A* and *B* site, respectively, such as $PbTiO_3$ (PT) [17], $BaTiO_3$ [18], or $BiFeO_3$ [19], possess a high crystallographic symmetry structure (*P4mm* or *R3c*) and ordered polarization in a long range, as shown on the left of Fig. 1. Ceramics with this kind of polarization configuration usually show quite a poor piezoresponse due to the limited rotation of polarization. When one or two other elements are added by chemical substitution, like PZT or PNN-PT, the symmetry of the system lowers and the constrain for some stable polarizations can be removed, leading to deviation of some polarizations away from the direction of high crystallographic symmetry, along with the enhanced piezoelectric response [11,15], as shown in the middle of Fig. 1. In this sense, when further increasing the types of the elements at the *B* site, the substitution atoms would certainly increase the distortions of Pb or other cations and modify the local polarization configuration correspondingly. This could further decrease the constrain of crystallographic symmetry, allowing the polarization to be aligned in diverse directions and resulting in a flexible polarization configuration, as shown on the right of Fig. 1. This concept shares more or less similar characteristics with the second generation high-entropy alloys, where more than four principal elements reside at one Wyckoff position in a system to increase the degree of randomness of the solid solution [20–22]. Noteworthily, the polarization orientation on the right of Fig. 1 is similar to that of the monoclinic phase, which has been proven to possess high flexibility [23,24]. Thus, via the multi-element substitution, a highly flexible polarization configuration that benefits the high piezoelectricity can be expected. Furthermore, it is worth mentioning that, due to the complex interaction among the *A, B*-site, and oxygen atoms in a perovskite structure, the polarization configuration of the Pb-based multi-element piezoelectrics remains elusive. Demonstrating the polarization configuration of high-performance multi-element piezoelectrics at the atomic scale is also of great scientific importance, which could boost the discovery and development of high-performance piezoelectrics.

Herein, via the design method called high-entropy piezoelectrics (HEPs), we systematically designed eleven kinds of new Pb-based high-performance piezoelectrics with highly flexible polarization configurations, in which the highest d_{33} of 1210 pC/N has been achieved. The structure and behavior of the special flexible polarization configuration were unambiguously revealed by the combination of *in-situ* high-energy synchrotron X-ray diffraction (SXRD), spherical aberration-corrected scanning transmission electron microscope (C_s-corrected STEM), and first-principles density functional theory (DFT) calculations. Based on systematic experimental and theoretical studies, we revealed the origin of this unique flexible polarization configuration and its critical role in improving the piezoelectric properties and built up connections among the number of *B*-site cations, polarization configuration, and piezoelectric performance in multi-element piezoelectric systems. The strategy developed in this work could be widely applicable for the design of numerous functional materials that have a strong structure-to-property correlation, which would boost the discovery and development of high-performance materials.

2. Experimental

The ceramics were prepared by conventional solid-state reaction [16,25]. The raw powders are high-purity PbO (99.9%), NiO (99.9%), Nb_2O_5 (99.9%), In_2O_3 (99.9%), Sc_2O_3 (99.9%) Yb_2O_3 (99.9%),

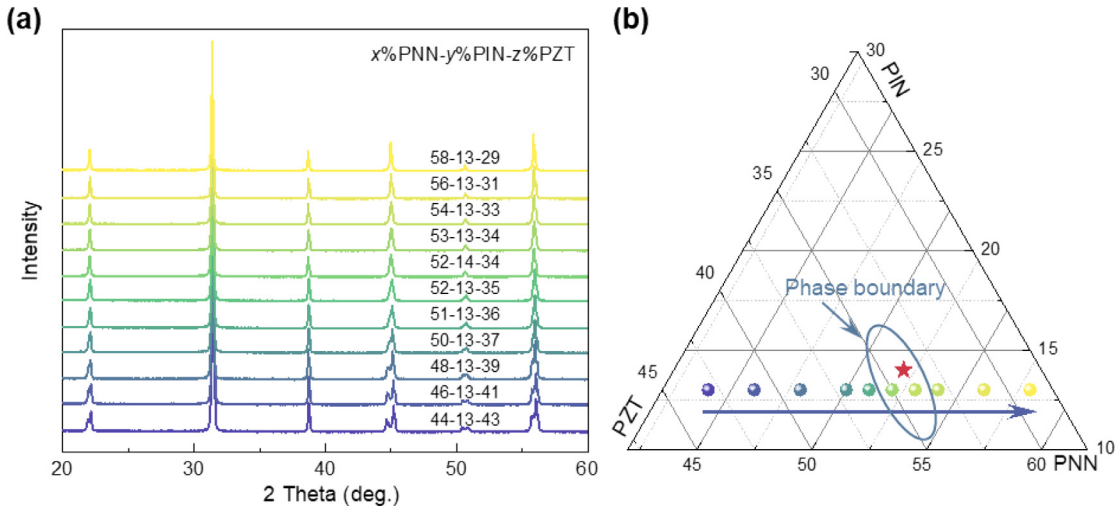

Fig. 2. Crystal structure of PNIZTN. (a) XRD pattern of the x%Pb($Ni_{0.33}Nb_{0.67}$)O_3-y%Pb($In_{0.5}Nb_{0.5}$)O_3-z%Pb($Zr_{0.1}Ti_{0.9}$)O_3 system, indicating the variation from T to R phase. (b) Relevant position in a ternary phase diagram.

ZrO_2 (99.9%), HfO_2 (99.9%), and TiO_2 (99%) powders. These oxide powders were weighed according to the stoichiometric ratio of the relevant designed materials. It should be noted that the PbO was weighted stoichiometrically with an excess of 1 wt% to compensate for the volatilization of PbO. For the simple piezoelectrics, the precursors are needed, such as Pb(In,Nb)O_3-$PbTiO_3$ (PIN-PT). The precursors, $NiNb_2O_6$, $InNbO_3$, $ScNbO_3$, and $YbNbO_3$ were prepared at 1000∼1100 °C for 6 h. Then, weighed powders were ball milled in a teflon can for 24 h with alcohol. The mixed slurry was dried in a drying oven for 4 h and put in an Al_2O_3 crucible. The crucible was then calcined at 850 °C for 5 h. Subsequently, the calcined powder was ball milled again same as the first ball milling and the slurry was also dried again. The dried powder was ground with 5 wt% polyvinyl alcohol (PVA) and then pressed into pellets with a diameter of 10 mm and thickness of 1.2 mm. The pellets are buried with the remanent powders in an Al_2O_3 crucible. The pellets were first sintered at 550 °C for 3 h to eliminate the PVA and then sintered at 1150∼1250 °C for 2 h to acquire the compact pellets. The fine sintered pellets were polished and sputtered with the gold electrode for performance measurement.

The phase structure of obtained ceramic powder was identified by laboratory X-ray diffraction (XRD, PANalytical, X'Pert PRO, Netherlands). The dielectric curves as a function of temperature were measured with a multi-frequency inductance capacitance resistance (LCR) meter (E4980, Agilent, Santa Clara, CA) at 0.5 V. The polarization-electric field (P-E) loops and strain-electric field (S-E) curves were measured with a ferroelectric analyzer (TF Analyzer 1000, aixACCT Systems GmbH, Germany) under the cyclic electric field of 1 Hz. For the measurement of piezoelectric property, the gold electrode sputtered pellets were first poled under a unidirectional electric field of 3 kV/mm, and then the small-signal d_{33} was measured with a quasi-static d_{33} meter (ZJ-3, China Academy of Acoustics). Atomic-scale high angle annular dark-field (HAADF)-STEM imaging was carried out on a 300 kV aberration-corrected FEI Titan Themis G2 microscope equipped with an X-FEG gun, monochromator, and double aberration correctors. The convergent semi-angle is 25 mrad for STEM. The collection angle is 48 to 200 mrad for HAADF and 12 to 45 mrad for ABF, respectively. *In-situ* electric field SXRD was performed at 11-ID-C beamline (λ=0.1173 Å, 105.9 keV) of the Advanced Photon Source (APS), and the 2D diffraction data were recorded by the PerkinElmer amorphous silicon area detector.

3. Results and discussion

3.1. Design of high-performance piezoelectrics

To achieve as high piezoelectricity as possible, the design of the multi-element piezoelectrics generally follows two rules. Firstly, the A-site atoms remain unchanged (Pb atom) for the controlling variable and the B-site atoms are chosen from those commonly used ones in piezoelectrics, such as Ni, Mg, *Sc*, Yb, In, Zr, Hf, Ti, and Nb. Secondly, the B-site atoms are chosen to contain as more as possible of the valence state and radius of cations. Considering that the number of possible compositions increases exponentially with the increase of B-site atoms kinds, the types of B-site atoms are chosen as four and five types. After choosing the element types, the composition is carefully optimized. Taking Pb(Ni,In,Zr,Ti,Nb)O_3 as an example, a series of components are synthesized and examined by XRD. As shown in Fig. 2a, all studied samples show a pure perovskite structure, indicating that the various B-site elements enter into the perovskite lattice. The characteristic {200} peaks of various components indicate an R-T phase boundary (Fig. 2a), the position of which is shown in a ternary phase diagram in Fig. 2b. The optimized nominal composition is marked as a red star in Fig. 2b. Thus, one kind of high-performance multi-element piezoelectrics is designed and the specifically optimized nominal composition of Pb(Ni,In,Zr,Ti,Nb)O_3 systems is determined as Pb($Ni_{0.173}In_{0.07}Zr_{0.034}Ti_{0.306}Nb_{0.417}$)$O_3$. Hereafter, we use PNIZTN to represent this specific composition.

3.2. Enhanced piezoelectric performance by enhancing entropy

Followed by the design method, eleven kinds of new high-performance piezoelectrics systems are systematically designed, and the relevant optimized compositions of each system are listed in Table S1. Noteworthily, all the optimized compositions of designed piezoelectrics possess high piezoelectric performance with d_{33} > 800 pC/N, among which ultrahigh d_{33} can reach ∼1200 pC/N in PNIZTN and ∼1210 pC/N in Pb($Ni_{0.177}Sc_{0.015}In_{0.06}Ti_{0.32}Nb_{0.428}$)$O_3$ (PNSITN) after the hot pressing sintering process. The d_{33} values of these newly designed quaternary (n_B = 4, n_B is the number of B-site elements types) and quinary (n_B = 5) HEPs together with typical Pb-based piezoelectrics investigated previously (specific compositions see Table S1 in Supplementary materials) are summa-

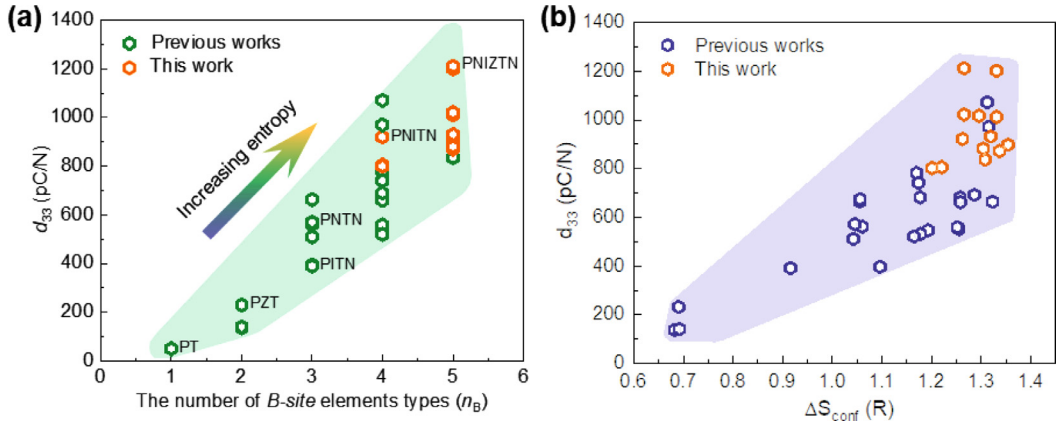

Fig. 3. Piezoelectric performance of designed materials. (a) Strong correlation between the piezoelectric performance (d_{33}) and the number of *B*-site element types (n_B) for a series of $PbBO_3$-based solid solutions. Details of d_{33} and compositions are listed in Table S1 and Fig. S1. (b) Piezoelectric properties (d_{33}) as a function of the relevant configurational entropy (ΔS_{conf}).

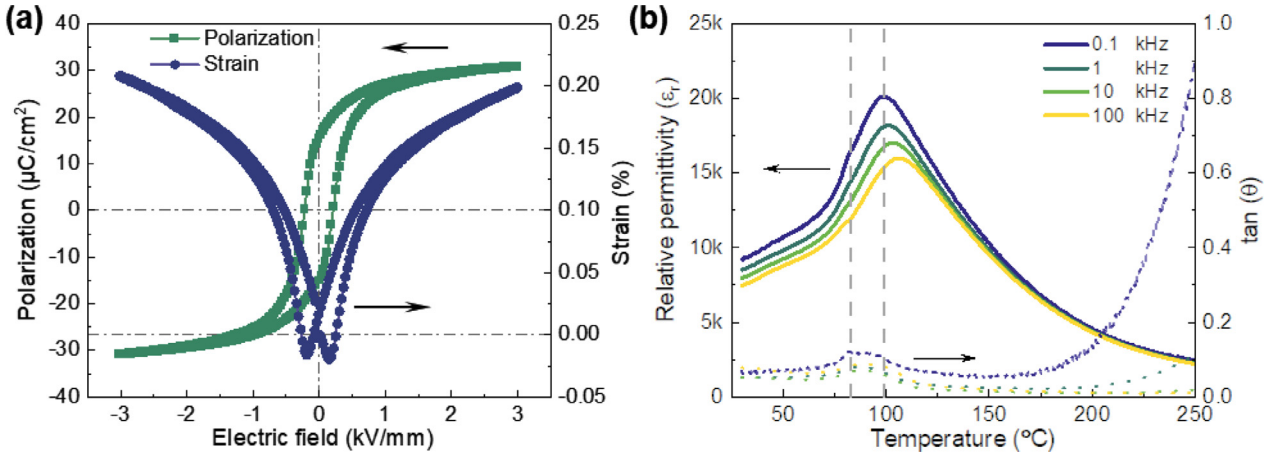

Fig. 4. Strain and dielectric properties of PNIZTN HEPs. (a) *P-E* and *S-E* curves of PNIZTN HEPs. (b) Temperature-dependent relative permittivity of the poled PNIZTN HEPs. The relevant depolarization and dielectric peak temperatures are 82 °C and 98 °C, respectively.

rized and drawn as a function of n_B in Fig. 3a. It is found that the average d_{33} values of each n_B system are gradually enhanced by increasing varieties of *B*-site elements, as expected. This tendency is consistent with our design idea shown in the schematic in Fig. 1, that is, the more types of *B*-site elements, the higher the piezoelectric performance.

Following the practice in the second generation high-entropy alloys [20–22], we refer to this concept of increasing the diversity of constituent elements of piezoelectrics for the design of high-performance piezoelectrics as the HEPs strategy. Therefore, the configurational entropy of materials in Fig. 3a is also calculated in Fig. 3b (see details in Supplementary materials). It can be seen that with the increase in the configurational entropy piezoelectric coefficient increases, manifesting an evident positive correlation. Note that the configurational entropy also shows dependence on the composition since for the same n_B the configurational entropy can be different. This suggests a strong correlation between the configurational entropy and the piezoelectric performance, confirming the reasonability of the concept of HEPs.

Generally, high-performance piezoelectrics also show good ferroelectric and dielectric properties. Thus, we also investigated the ferroelectric and dielectric properties of the PNIZTN ceramic in Fig. 4. The small negative strain in strain versus electric field (*S-E*) curve (Fig. 4a) demonstrates that there is a little macro domain switching during the cyclic electric field applying process, suggesting the small size of domains. This is double confirmed by the frequency dispersion of the temperature dependence relative permittivity curve shown in Fig. 4b. These results indicate that PNIZTN is a classical relaxor ferroelectric with the small size domains. The T_m value under the 0.1 kHz measurement voltage is 98ºC. This low T_m value indicates the small lattice parameters anisotropy and weak long-range ferroelectric order, which is commonly accompanied by the high flexible polarizations. The relative permittivity at room temperature is above 9000 under the 0.1 kHz measurement voltage. The high relative permittivity indicates that the polarization can be easily switched by a small stimulated electric field. These phenomena suggest that the domains of PNIZTN are small in size and the polarization possesses relatively high flexibility.

3.3. Local polarization configurations

To look into the structure of the polarization configuration of PNIZTN and the microscopic origin of this high piezoelectricity, the polarization distributions of PNIZTN HEPs were investigated at the atomic scale by C_s-corrected STEM. Atomically resolved HAADF-STEM images were acquired at ⟨100⟩ zone axis and quantitatively analyzed in Fig. 5. Fig. 5a shows a typical HAADF-STEM image, in which atomic columns were fitted to get their intensities and atomic positions (Figs. S2 and S3) [26]. Based on fitted positions, atomic polarization displacements were calculated and mapped (Fig. S3). The polarization configuration can be clearly seen by the smooth color transition in the contour map of the polarization an-

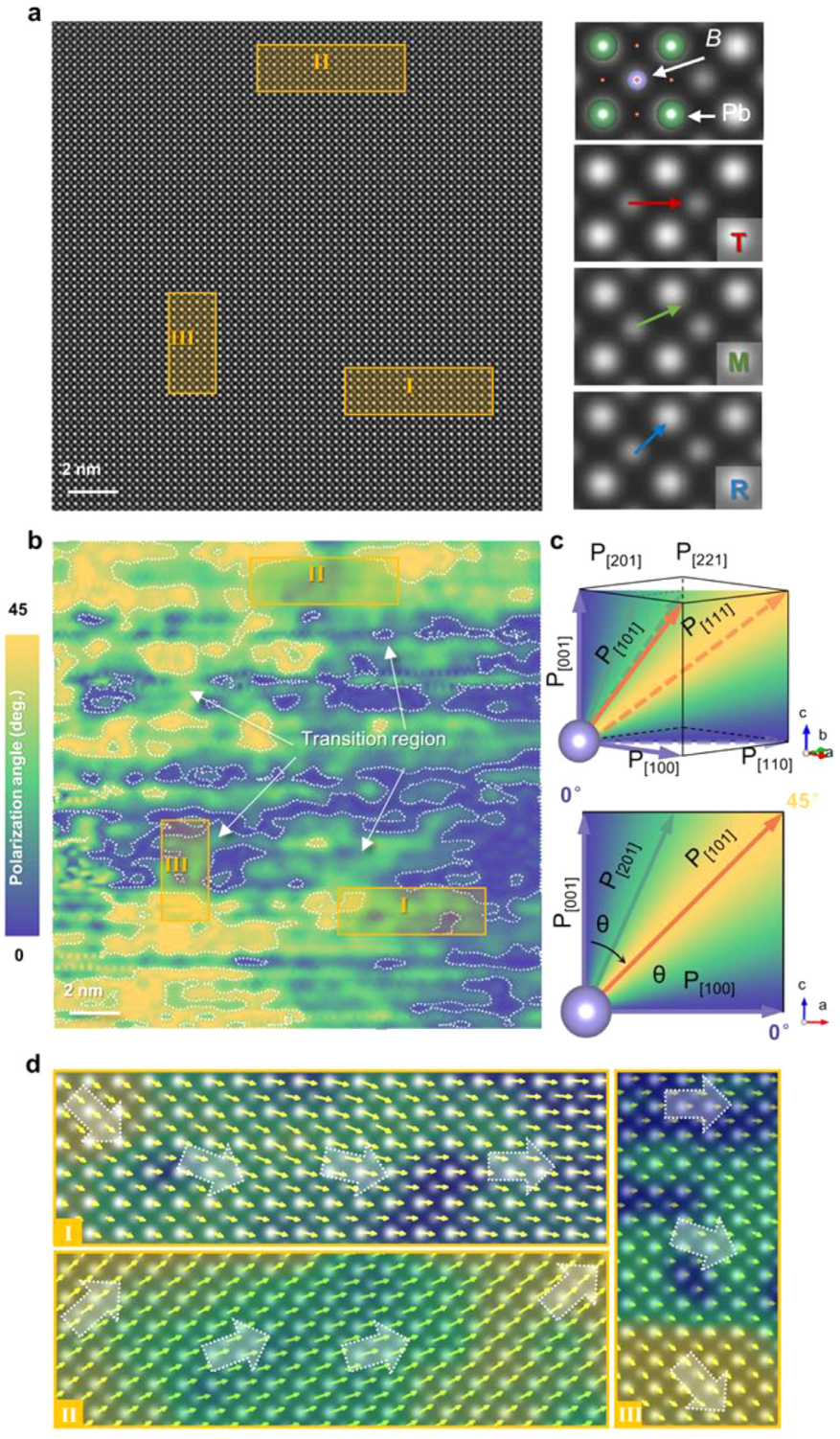

Fig. 5. Atomic resolution polarization distribution of PNIZTN HEPs. (a) HAADF-STEM image of PNIZTN HEPs at the ⟨100⟩ zone axis overlaid with polarization displacement vectors (yellow arrows). (b) Contour map of the distribution of polarization angle (θ) in (a). (c) Schematic of the distribution of θ in a pseudocubic unit cell and relevant projection plane. (d) Enlargements of the marked regions in (a), showing continuous evolution of polarization vectors.

gle (θ) (Fig. 5b). It should be noted that to highlight the evolution characteristics of vectors, θ has been converted into the range from 0° (T phase) to 45° (R phase) according to the symmetry of the unit cell and the projection direction of the image (Fig. 5c). As shown in the enlargements of selected regions (Fig. 5b), polarization vectors characterize a continuous evolution between ⟨001⟩ and ⟨111⟩ directions, manifesting the significantly lowered local crystallographic symmetry and high flexibility. Hence, the large scale of transitional regions (green color) that spread out over the whole area in Fig. 5b indicates the flexibility of this unique polarization configuration.

This scenario is markedly different from that in classic piezoelectrics at MPB, where the polarizations are confined in limited directions, like ⟨100⟩ and ⟨111⟩, within isolated nanodomains of

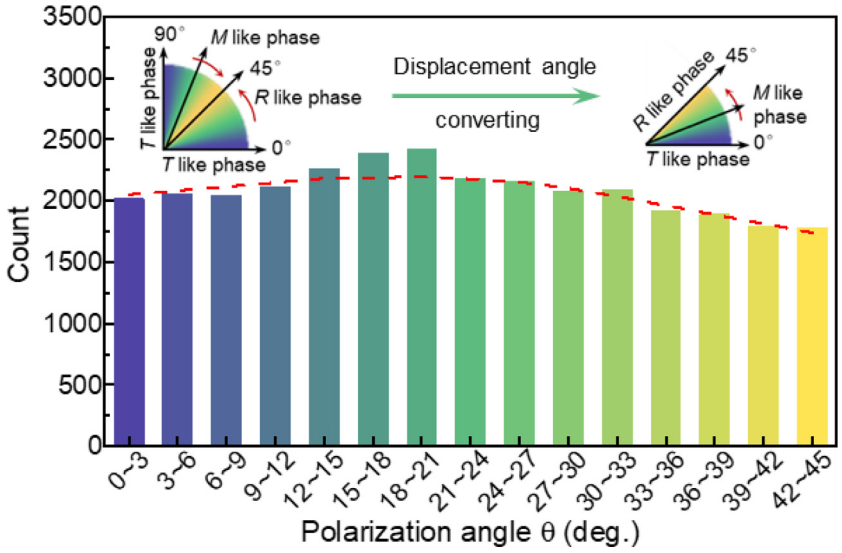

Fig. 6. Statistics of the distribution of θ in the range of 0°−45°, extracted from over 30,000 polarization vectors. The red dashed curve indicates the even distribution of θ over the whole angle range. Inset shows the conversion from 0°–90° to 0°–45°.

T and *R* phases [3,4,27]. The continuously transitional polarization configuration in this work breaks the constrain of crystallographic symmetry, which benefits the rotation of the polarization. The more transitional regions in material, the more easily the polarizations can rotate. Statistically, over 30 thousand vectors were quantitatively analyzed to acquire the distributions of polarization angles. The results show an almost even distribution of angles in the whole range of 0–45°, as demonstrated in Fig. 6. It is worth mentioning that the monoclinic phase with a fixed polarization θ in the range of 0–45° has been determined by synchrotron XRD results around phase boundaries in many previous studies [24,28-30], which is considered the bridge for polarization reorientation and the primary origin of high piezoelectric effect. The unique polarization configuration found in this work can be considered as the coexistence of many monoclinic phases with different θ values at the atomic scale, suggesting the enhanced flexibility of the polarization response under an external field. Such a flexible polarization configuration should originate from the local structural distortions introduced by the disparate ion radiuses and ferroelectricity activities of different *B*-site cations in HEPs, as shown in Fig. 1. This eventually results in the significantly enhanced flexibility of polarization in our case, as demonstrated above, which provides a basis for the higher piezoelectric response of HEPs. These experimental observations are well consistent with our design idea (Fig. 1) and previous theoretical studies that the increased disorder degree of the *B* site would construct multi-type local distortions of Pb cations, thus leading to a more chaotic state of local ferroelectric polarization [31,32].

Using *in-situ* high-energy SXRD (Fig. 7), the behavior of this flexible polarization configuration under external electric fields was investigated to directly correlate it with the macroscopic piezoelectric property. Commonly, the one-dimension (1D) XRD patterns are integrated from the diffraction pattern sectors of 15° in two-dimension (2D) XRD patterns [33], and the azimuthal angles of each sector are shown in Fig. 7. Fig. 8a shows the electric field dependence of the {111} and {200} peaks at the 0° sector for the poled PNIZTN HEPs. During the whole loading-unloading process, the {111} and {200} peaks remain almost a single peak without detectable splitting, as shown in Fig. 8a. Besides, the full width at half maximums (HWHM) of the integrated {200} peaks is almost the same over all azimuthal angles for both unpoled and E_{max} states (Fig. 8b). These indicate the tiny anisotropy of the crystal

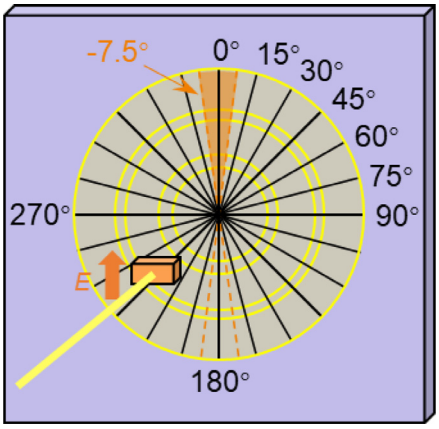

Fig. 7. Schematic of in-situ high-energy synchrotron X-ray diffraction (SXRD) and relevant azimuthal angle setting.

structure, which is consistent with the flexible nature of polarizations (Fig. 6). By carefully fitting the {200} peak, the electric field dependence of lattice strain can be acquired (Fig. 8c).

Generally, the piezoelectric performance arises from the factors such as intrinsic lattice strain, domain switching, and phase transition [34–36]. To reveal the dominant factor for this flexible polarization configuration in HEPs, the lattice strain of {200} is compared with the measured bipolar macro strain. As shown in Fig. 8c, the intrinsic lattice strain is nearly the same as the macro strain, suggesting that the high piezoelectric performance should mainly originate from the intrinsic lattice strain. This can be further confirmed in Fig. 8d by checking the electric field-dependent behaviors of asymmetry parameter [37] and HWHM of {200} peak, which change sensitively with domain switch or phase transition [38,39]. Being almost invariable of both profile parameters for {200} peak with electric fields suggests the dominative role of intrinsic lattice strain in the high piezoelectricity of HEPs. This result is similar to the one of the monoclinic phase, in which the intrinsic lattice strain plays the primary role in the high piezoelectricity [33,40]. This suggests the polarization in the transition regions is responsible for the high performance of HEPs. Combining *in-situ* SXRD results with microscopy observations, a clear picture

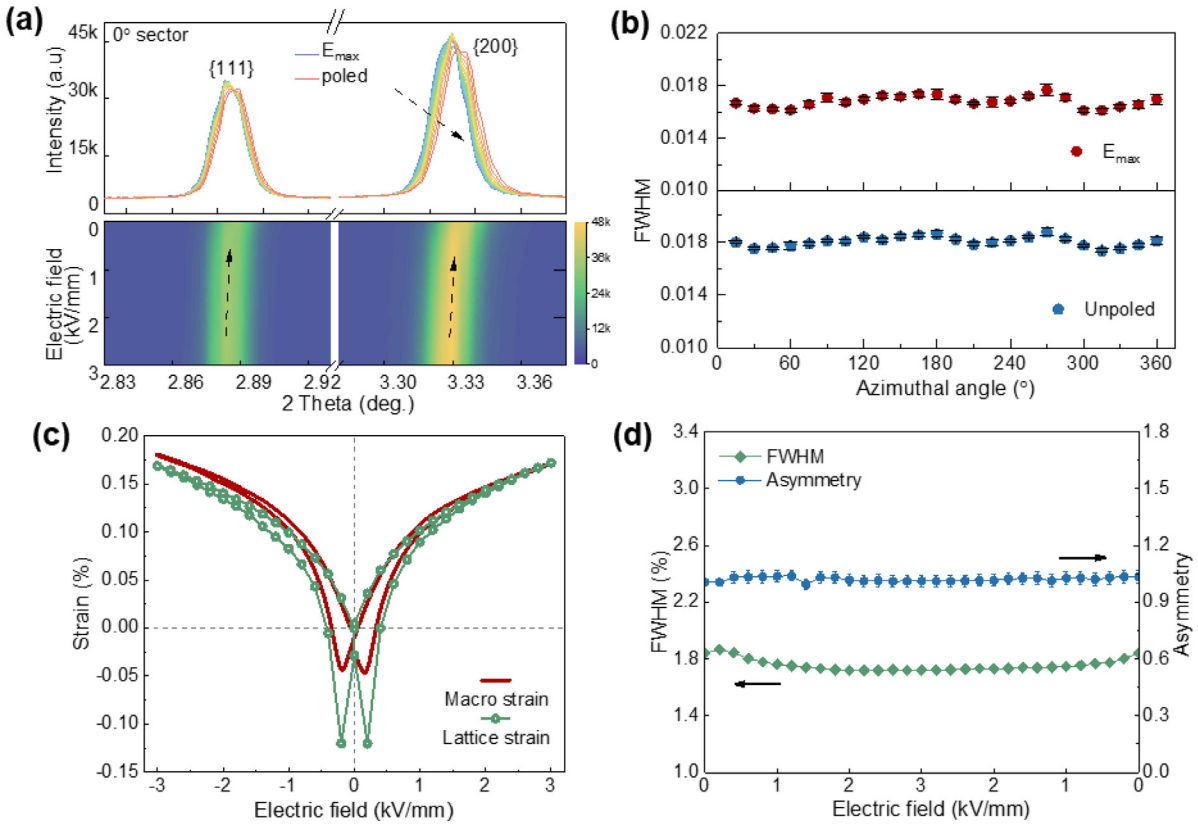

Fig. 8. In-situ high-energy synchrotron X-ray diffraction of PNIZTN HEPs. (a) Evolution of {111} and {200} peaks at 0° sector as a function of electric field. {111} and {200} peaks shift to a higher angle without peak splitting upon unloading the electric field. Arrows indicate the direction of the unloading electric field. (b) FWHM of {200} peaks as a function of azimuthal angle under the state of E_{max} (upper) and unpoled (lower). (c) Comparison of bipolar macro strain and {200} lattice strain. (d) Evolution of FWHM and asymmetry for the {200} peak as a function of the electric field.

of how the flexible polarization configuration can introduce high piezoelectricity can be acquired in HEPs. Due to the tiny anisotropy of lattice and little constraint from the neighbors, local polarizations in various directions can rotate easily and flexibly upon loading external electric fields. The simultaneous and synergistic rotation of the evenly distributed polarizations will enhance the intrinsic lattice strain and eventually lead to high piezoelectricity in HEPs.

To understand the intrinsic origin of this unusual flexible polarization configuration, we further performed DFT calculations on HEPs. To get statistically meaningful descriptions of local structural features, we consider 30 different arrangements of *B*-site cations in a 3 × 3 supercell (Fig. 9a) for the systems of PZT, PITN, PNIZTN (see calculation details in Supplementary materials). The angles between the projective components of local displacement and the relevant coordinate axes (Fig. 9b) are counted for comparison with the observed statistical result of polarization angles. As shown in Figs. 9c and 9d, with the increase of the species of *B*-site cations, distributions of local displacement magnitudes of *A*-site Pb cations and *B*-site cations become more and more randomly. Meanwhile, local displacement angles (θ') become more and more evenly distributed with the increase of the species of *B*-site cations, as indicated in Fig. 9e, showing good consistency with the experimental statistic results in Fig. 6. These calculation results verify that multiple *B*-site atoms can indeed enhance the flexibility of polarizations.

Furthermore, the distribution of the local displacement magnitude is qualified and correlated with d_{33} in Fig. 10. Following the "3σ rule" (see detailed definition in Supplementary materials), quantitative parameters of the characteristic width (Δ_{Pb} for Pb, Δ_B for *B*-site cations) are defined and drawn in Fig. 10. Overall, both characteristic widths show a positive correlation with n_B, except for a slight decrease of Δ_B in the PNIZTN. This indicates that the magnitudes of local displacements of both *A*-site and *B*-site ions become increasingly dispersive with increasing n_B in piezoelectrics. The large local displacement offers large polarization, and the small displacement possesses high flexibility, eventually leading to the high piezoelectric performance. The "softness" of local potential energy around each Pb atom ($\langle k \rangle$) is also quantified by computing the change in energy with respect to small perturbations (the definition is described in Methods). $\langle k \rangle$ represents the easiness of Pb movement in response to external stimuli such as electric/stress fields. That is, smaller $\langle k \rangle$ corresponds to the higher intrinsic lattice response and larger d_{33}. As shown in Fig. 10, $\langle k \rangle$ drops with the increase of n_B. This suggests that the lattice can respond easier to the electric field with increasing n_B, which also indicates the enhanced flexibility of polarizations.

Why the flexible polarization configuration is beneficial for high piezoelectricity can also be understood from the thermodynamic perspective. Since polarizations are evenly distributed and the anisotropy of lattice is tiny in the polarization configuration, the free energies of polarizations with different angles are quite similar. That the disordered *B*-site atoms result in a flatted free energy profile has also been reported in $Pb(Sc_{0.5}Nb_{0.5})O_3$ systems [41]. Therefore, according to the reported thermodynamic calculation the flat Gibbs free energy profile is generally preferred for the improvement of piezoelectric response [42], the flat Gibbs free energy profile in the flexible polarization configuration benefits the polarization rotation leading to high piezoelectric performance.

Additionally, in terms of the design of new HEPs, plenty of potential high-performance systems are available since the number of possible compositions increases exponentially with increasing n_B. In future studies, the high-throughput screening method can be

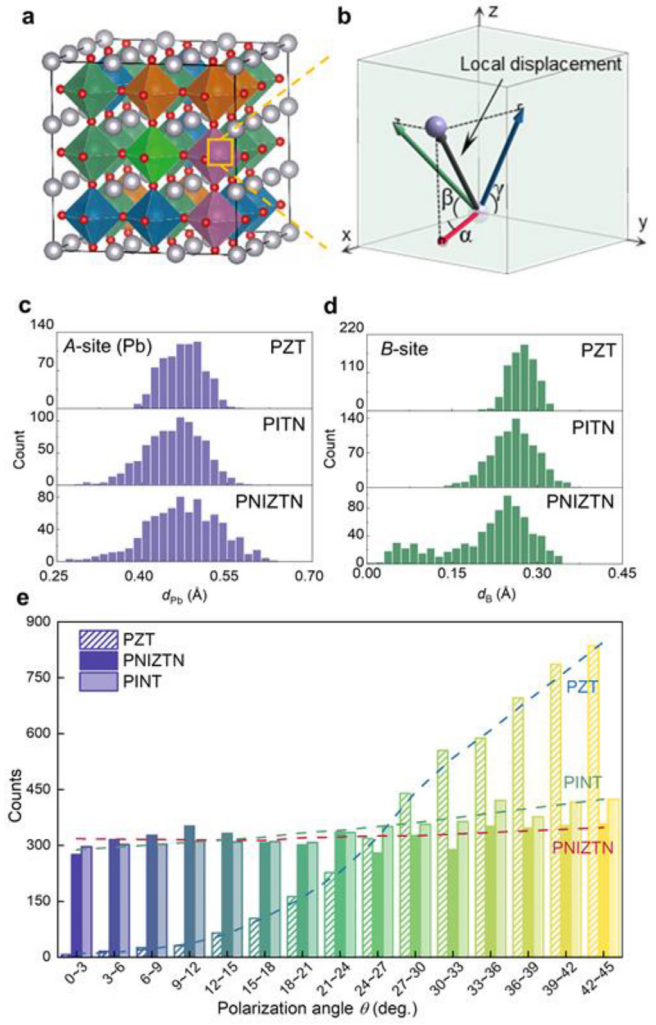

Fig. 9. Origin of flexible polarization configuration by first principles calculation. (a) Representative 3 × 3 supercells of PNIZTN for the first-principles calculation modeling. (b) Schematic of the projection of the local displacement vector. Displacement vector angle is defined as the one between the coordinate axis and the relevant projective component. (c, d, e) Statistics of magnitudes (c, d) and angles (e) of local polarization displacements of Pb and *B*-site cations in PZT, PITN, PNIZTN considering thirty kinds of arrangements of *B*-site atoms in a 3 × 3 supercell.

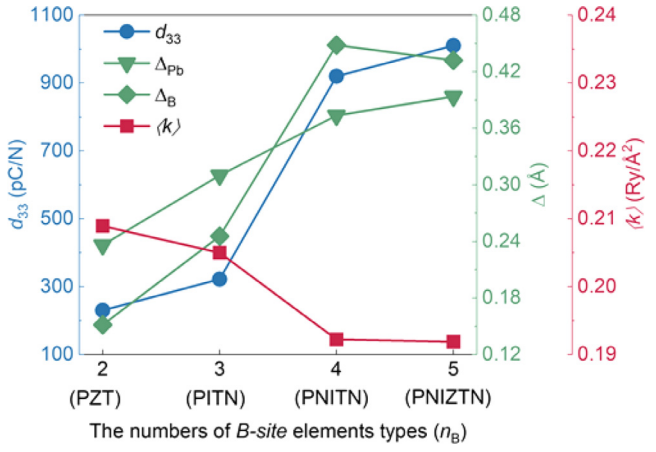

Fig. 10. Correlation between d_{33} and the degree of disordering represented by the local displacement of ions (Δ) and susceptibility (⟨*k*⟩).

developed to boost the exploration of high-performance HEPs. It is worth mentioning that since we only roughly explore the phase diagram of each system, higher piezoelectric performance could be expected in the HEPs if the optimization of chemical composition can be fully carried out.

4. Conclusions

The present work systematically designs and synthesizes three new kinds of quaternary HEPs and eight new kinds of quinary HEPs with ultrahigh piezoelectricity through increasing the diversities of *B*-site elements in piezoelectrics. A giant d_{33} of 1200 pC/N has been achieved, which has unique continuously orientated polarizations. This polarization configuration is highly flexible and has been proven to benefit the high piezoelectric performance. Then, the DFT calculations further clarify the intrinsic origin of this unique flexible polarization configuration and large lattice response, in which the increased elemental diversity can result in the dispersive distribution of local *A*- and *B*-site atoms and the softness of each Pb atom. Thus, with these experimental and theoretical results, the unique polarization configuration of multi-element Pb-based piezoelectric is clearly illustrated and the approach to design these high-performance piezoelectrics could offer guidance and new opportunities for further enhancing the piezoelectric properties based on the present piezoelectrics, as well as other functional materials.

Declaration of Competing Interest

The authors declare that they have no known competing financial interests or personal relationships that could have appeared to influence the work reported in this paper.

Acknowledgments

This work was supported by the National Natural Science Foundation of China (Grant Nos. 21825102, 2211101063, 22001014, and 52172181), National Postdoctoral Program for Innovative Talents (BX20200043 and BX20200044), the China Postdoctoral Science Foundation (Grant No. 2021M690366), the Fundamental Research Funds for the Central Universities, China (Grant No. 06500145), and State Key Laboratory of New Ceramic and Fine Processing Tsinghua University (Grand No. KF202110). This research made use of the resources of the Beijing National Center for Electron Microscopy at Tsinghua University and resources of the Advanced Photon Source, a US Department of Energy (DOE) Office of Science User Facility operated for the DOE Office of Science by Argonne National Laboratory under Contract No. DE-AC02–06CH11357.

Supplementary materials

Supplementary material associated with this article can be found, in the online version, at doi:10.1016/j.actamat.2022.118115.

References

[1] B. Jaffe, R.S. Roth, S. Marzullo, Piezoelectric properties of lead zirconate-lead titanate solid-solution ceramics, J. Appl. Phys. 25 (6) (1954) 809–810.
[2] W. Liu, X. Ren, Large Piezoelectric Effect in Pb-Free Ceramics, Phys. Rev. Lett. 103 (25) (2009) 257602.
[3] H. Tao, H. Wu, Y. Liu, Y. Zhang, J. Wu, F. Li, X. Lyu, C. Zhao, D. Xiao, J. Zhu, S.J. Pennycook, Ultrahigh performance in lead-free piezoceramics utilizing a relaxor slush polar state with multiphase coexistence, J. Am. Chem. Soc. 141 (35) (2019) 13987–13994.
[4] F. Li, D. Lin, Z. Chen, Z. Cheng, J. Wang, C. Li, Z. Xu, Q. Huang, X. Liao, L.-Q. Chen, T.R. Shrout, S. Zhang, Ultrahigh piezoelectricity in ferroelectric ceramics by design, Nat. Mater. 17 (4) (2018) 349–354.
[5] S.W. Choi, R.T.R. Shrout, S.J. Jang, A.S. Bhalla, Dielectric and pyroelectric properties in the $Pb(Mg_{1/3}Nb_{2/3})O_3$-$PbTiO_3$ system, Ferroelectrics 100 (1) (1989) 29–38.

[6] T. Takenaka, K.-i. Maruyama, K. Sakata, $(Bi_{1/2}Na_{1/2})TiO_3$-$BaTiO_3$ system for lead--free piezoelectric ceramics, Jpn. J. Appl. Phys. 30 (Part 1, No. 9B) (1991) 2236–2239.

[7] M.M. Kumar, A. Srinivas, S.V. Suryanarayana, Structure property relations in $BiFeO_3$/$BaTiO_3$ solid solutions, J. Appl. Phys. 87 (2) (2000) 855–862.

[8] S.E. Park, T.R. Shrout, Ultrahigh strain and piezoelectric behavior in relaxor based ferroelectric single crystals, J. Appl. Phys. 82 (4) (1997) 1804–1811.

[9] Y. Dai, X. Zhang, G. Zhou, Phase transitional behavior in $K_{0.5}Na_{0.5}NbO_3$-$LiTaO_3$ ceramics, Appl. Phys. Lett. 90 (26) (2007) 262903.

[10] J. Wu, Advances in Lead-Free Piezoelectric Materials, Springer, 2018.

[11] D. Vanderbilt, M.H. Cohen, Monoclinic and triclinic phases in higher-order Devonshire theory, Phys. Rev. B 63 (9) (2001) 094108.

[12] D. Corker, A. Glazer, R. Whatmore, A. Stallard, F. Fauth, A neutron diffraction investigation into the rhombohedral phases of the perovskite series, J. Phys. 10 (28) (1998) 6251.

[13] N. Zhang, H. Yokota, A.M. Glazer, Z. Ren, D.A. Keen, D.S. Keeble, P.A. Thomas, Z.G. Ye, The missing boundary in the phase diagram of $PbZr_{1-x}TixO_3$, Nat. Commun. 5 (1) (2014) 5231.

[14] B. Noheda, D.E. Cox, G. Shirane, S.E. Park, L.E. Cross, Z. Zhong, Polarization rotation via a monoclinic phase in the piezoelectric 92%$PbZn_{1/3}Nb_{2/3}O_3$-8%$PbTiO_3$, Phys. Rev. Lett. 86 (17) (2001) 3891–3894.

[15] B. Noheda, D. Cox, Bridging phases at the morphotropic boundaries of lead oxide solid solutions, Phase Trans. 79 (1–2) (2006) 5–20.

[16] Q.H. Guo, L.T. Hou, F. Li, F.Q. Xia, P.B. Wang, H. Hao, H.J. Sun, H.X. Liu, S.J. Zhang, Investigation of dielectric and piezoelectric properties in aliovalent Eu^{3+}-modified $Pb(Mg_{1/3}Nb_{2/3})O_3$-$PbTiO_3$ ceramics, J. Am. Ceram. Soc. 102 (12) (2019) 7428–7435.

[17] R.J. Nelmes, W.F. Kuhs, The crystal structure of tetragonal $PbTiO_3$ at room temperature and at 700K, Solid State Commun 54 (8) (1985) 721–723.

[18] R.H. Buttner, E.N. Maslen, Structural parameters and electron difference density in $BaTiO_3$, Acta Crystallogr. Sect. B: Struct. Sci. 48 (6) (1992) 764–769.

[19] J.M. Moreau, C. Michel, R. Gerson, W.J. James, Ferroelectric $BiFeO_3$ X-ray and neutron diffraction study, J. Phys. Chem. Solids 32 (6) (1971) 1315–1320.

[20] Z. Li, K.G. Pradeep, Y. Deng, D. Raabe, C.C. Tasan, Metastable high-entropy dual-phase alloys overcome the strength-ductility trade-off, Nature 534 (7606) (2016) 227–230.

[21] Y. Lu, X. Gao, L. Jiang, Z. Chen, T. Wang, J. Jie, H. Kang, Y. Zhang, S. Guo, H. Ruan, Y. Zhao, Z. Cao, T. Li, Directly cast bulk eutectic and near-eutectic high entropy alloys with balanced strength and ductility in a wide temperature range, Acta Mater 124 (2017) 143–150.

[22] W. Zhang, P.K. Liaw, Y. Zhang, Science and technology in high-entropy alloys, Sci. China Mater. 61 (1) (2018) 2–22.

[23] H. Fu, R.E. Cohen, Polarization rotation mechanism for ultrahigh electromechanical response in single-crystal piezoelectrics, Nature 403 (6767) (2000) 281–283.

[24] H. Liu, J. Chen, L. Fan, Y. Ren, Z. Pan, K.V. Lalitha, J. Rodel, X. Xing, Critical role of monoclinic polarization rotation in high-performance perovskite piezoelectric materials, Phys. Rev. Lett. 119 (1) (2017) 017601.

[25] J. Du, J. Qiu, K. Zhu, H. Ji, Enhanced piezoelectric properties of 0.55$Pb(Ni_{1/3}Nb_{2/3})O_3$-0.135$PbZrO_3$-0.315$PbTiO_3$ ternary ceramics by optimizing sintering temperature, J. Electroceram. 32 (2–3) (2014) 234–239.

[26] A.K. Yadav, C.T. Nelson, S.L. Hsu, Z. Hong, J.D. Clarkson, C.M. Schlepütz, A.R. Damodaran, P. Shafer, E. Arenholz, L.R. Dedon, D. Chen, A. Vishwanath, A.M. Minor, L.Q. Chen, J.F. Scott, L.W. Martin, R. Ramesh, Observation of polar vortices in oxide superlattices, Nature 530 (7589) (2016) 198–201.

[27] D. Wang, Z. Fan, G. Rao, G. Wang, Y. Liu, C. Yuan, T. Ma, D. Li, X. Tan, Z. Lu, A. Feteira, S. Liu, C. Zhou, S. Zhang, Ultrahigh piezoelectricity in lead-free piezoceramics by synergistic design, Nano Energy 76 (2020) 104944.

[28] J. Fu, H. Qi, A. Xie, A. Tian, R. Zuo, Understanding the correlation between intermediate monoclinic phase (*Cc*) and piezoelectric properties in $NaNbO_3$-$BaTiO_3$-$CaZrO_3$ ternary system with octahedral tilt, Acta Mater 215 (2021) 117100.

[29] R. Guo, L.E. Cross, S.E. Park, B. Noheda, D.E. Cox, G. Shirane, Origin of the High Piezoelectric Response in $PbZr_{1-x}Ti_xO_3$, Phys. Rev. Lett. 84 (23) (2000) 5423–5426.

[30] B. Noheda, Structure and high-piezoelectricity in lead oxide solid solutions, Curr. Opin. Solid State Mater. Sci. 6 (1) (2002) 27–34.

[31] I. Grinberg, V.R. Cooper, A.M. Rappe, Relationship between local structure and phase transitions of a disordered solid solution, Nature 419 (6910) (2002) 909–911.

[32] I. Grinberg, A.M. Rappe, First principles calculations, crystal chemistry and properties of ferroelectric perovskites, Phase Transitions 80 (4–5) (2007) 351–368.

[33] L. Fan, J. Chen, Y. Ren, Z. Pan, L. Zhang, X. Xing, Unique piezoelectric properties of the monoclinic phase in $Pb(Zr,Ti)O_3$ ceramics: large lattice strain and negligible domain switching, Phys. Rev. Lett. 116 (2) (2016) 027601.

[34] H. Liu, J. Chen, H. Huang, L. Fan, Y. Ren, Z. Pan, J. Deng, L.Q. Chen, X. Xing, Role of reversible phase transformation for strong piezoelectric performance at the morphotropic phase boundary, Phys. Rev. Lett. 120 (5) (2018) 055501.

[35] L. Bellaiche, D. Vanderbilt, Intrinsic piezoelectric response in perovskite alloys: PMN-PT versus PZT, Phys. Rev. Lett. 83 (7) (1999) 1347–1350.

[36] J.L. Jones, E. Aksel, G. Tutuncu, T.-.M. Usher, J. Chen, X. Xing, A.J. Studer, Domain wall and interphase boundary motion in a two-phase morphotropic phase boundary ferroelectric: frequency dispersion and contribution to piezoelectric and dielectric properties, Phys. Rev. B 86 (2) (2012) 024104.

[37] J.E. Daniels, J.L. Jones, T.R. Finlayson, Characterization of domain structures from diffraction profiles in tetragonal ferroelastic ceramics, J. Phys. D 39 (24) (2006) 5294–5299.

[38] A. Pramanick, D. Damjanovic, J.E. Daniels, J.C. Nino, J.L. Jones, Origins of electro-mechanical coupling in polycrystalline ferroelectrics during subcoercive electrical loading, J. Am. Ceram. Soc. 94 (2) (2011) 293–309.

[39] S. Sun, Y. Zhang, L. Fan, S. Deng, B. Gao, Y. Ren, H. Liu, J. Chen, Role of tetragonal distortion on domain switching and lattice strain of piezoelectrics by in--situ synchrotron diffraction, Scripta Mater. 194 (2021) 113627.

[40] D. Hou, T.-.M. Usher, L. Fulanovic, M. Vrabelj, M. Otonicar, H. Ursic, B. Malic, I. Levin, J.L. Jones, Field-induced polarization rotation and phase transitions in 0.70$Pb(Mg_{1/3}Nb_{2/3})O_3$-0.30$PbTiO_3$ piezoceramics observed by in situ high-energy x-ray scattering, Phys. Rev. B 97 (21) (2018) 214102.

[41] J. Íñiguez, L. Bellaiche, Ab Initio design of perovskite alloys with predetermined properties: the case of $Pb(Sc_{0.5}Nb_{0.5})O_3$, Phys. Rev. Lett. 87 (9) (2001) 095503.

[42] D. Damjanovic, Contributions to the piezoelectric effect in ferroelectric single crystals and ceramics, J. Am. Ceram. Soc. 88 (10) (2005) 2663–2676.